NUMERICAL SOLUTION OF THE SAINT VENANT EQUATION FOR NON-NEWTONIAN FLUID

Cornelius E. Agu and Bernt Lie[1]
Faculty of Technology, Telemark University College
Norway

ABSTRACT

Non-Newtonian fluid flow through a Venturi channel is studied using the Saint Venant equation. The nonlinear hyperbolic equation is numerically tricky to solve, therefore in this study, we consider the finite volume method with staggered grids which we find suitable for control applications. Both steady state and dynamic solutions of the fluids with different rheological properties are simulated and analyzed. The purpose of this study is to develop a numerical algorithm for estimation of flow rate of a non-Newtonian fluid in an open channel. Because a non-Newtonian fluid flow is often associated with supercritical flow upstream, the standard subcritical flume may not be suitable for estimating the flow rate. This study reveals that when a sufficient contraction is introduced in a channel, the supercritical flow jumps to subcritical flow level and then passes through the critical depth at the throat while accelerating towards the channel end. With this flow transition, the study shows that in steady states a unique relationship can be established between the flow rate and the free surface level at the gauging point. The dynamic solution also shows that the system responds positively for a step change in the flow rate, reaching the steady state solution within the simulation run time.

Keywords: Venturi channel, Saint Venant equation, non-Newtonian fluid, Rheological properties, Finite volume method.

[1] Corresponding author, E-mail:bernt.lie@hit.no

NOMENCLATURE

A Cross sectional area [m^2]
$\bar{A}$ Average cross sectional area [m^2]
B Free surface top width [m]
b Channel width [m]
Fr Froude number
g Gravitational acceleration [m/s^2]
h Free surface level [m]
K Flow behaviour index [$Pa.s^n$]
L Length [m]
N Spatial grid size
n Fluid consistency index
P_{wet} Wetted perimeter [m]
Q Flow rate [m^3/s]
R_h Hydraulic radius [m]
S Slope
V Average velocity [m/s]
x Distance
$\boldsymbol{\alpha}$ Kinetic energy correction coefficient
β Momentum correction coefficient
$\boldsymbol{\rho}$ Density [kg/m^3]
θ Inclination of the channel bottom [degree]
$\boldsymbol{\tau_y}$ Yield shear stress [Pa]

Subscripts

0 Bottom origin; initial condition
c Critical
i Index in space
in Inlet
out Outlet

INTRODUCTION

Fluid flow in an open channel has wide industrial applicability. It is used in transportation of slurries, water supply for irrigation and river flow [1]. Due to severe operating conditions, use of common flow meters may be considered very expensive or unsafe to measure the flow rate of slurries (non-Newtonian fluids). One common and simple method is to use an open channel hydraulic structure such as a "weir" (Notch) or a "control flume" which introduces a restriction in the flow direction that results in flow variations (that is change in approach velocity and level) along the channel [2]. Flumes are commonly used in the industry. In homogeneous slurry transport, particle settling is not desired, and this requires that the flume used for the transport and flow measurement must be designed for supercritical flow conditions [3, 4]. The current flume design based on ISO 4359 standard is applied to subcritical upstream conditions [5], and this brings about this study. There has been some research on the requirements for supercritical flume design. A procedure for designing and using a supercritical flume where it is assumed that critical flow conditions occur at the entrance of the channel throat is outlined in [4].

The main purpose of this study is to develop a numerical scheme for estimating the flow rate of a non-Newtonian fluid in an open channel. To complete this task, one-dimensional Saint Venant equation is solved in both steady and unsteady states. One major drawback in the use of the model is that the unsteady 1-D Saint Venant equation is numerical difficult to solve [6]. Several techniques for solving the non-linear partial differential equations have been documented in recent research. One such scheme is based on finite volume method with a switch to energy head conservation model to ensure accuracy, especially in a rapid change in the channel width [7, 3]. Most of the schemes are based on finite different methods with or without staggered grids, and majority is suitable for subcritical flow conditions. Some methods used in supercritical conditions are based on shock-capturing approach or a classical scheme for solving compressible Euler equations [6]. The schemes especially those for supercritical and transition state are significantly computational demanding [6].

The present work focuses on the steady state solution of 1-D Saint Venant equation for a supercritical flow in a Venturi channel. In steady

state conditions, determining a model which uses only the free surface level measured at a specific point in the flow to estimate the flow rate is the main objective. A scheme for obtaining a solution for unsteady state model will also be covered. For unsteady state solution, the main idea is to ascertain the dynamic response of the system for a slight deviation in a steady state value. The scheme which will be based on the finite volume method is expected to be simple and suitable for control purposes.

In the following sections, the governing equations are presented, and the numerical scheme for steady state and unsteady state analyses are derived. The numerical solution is compared with a known solution from literature, and the model for flow rate estimation is then derived. Different results from the scheme are presented and discussed.

GOVERNING EQUATIONS

The unsteady state flow of fluid in an open channel can be described by the one-dimensional Saint Venant equations [6]:

$$\frac{\partial A}{\partial t} + \frac{\partial Q}{\partial x} = 0 \quad (1)$$

$$\frac{\partial Q}{\partial t} + \frac{\partial \left(\frac{\beta Q^2}{A}\right)}{\partial x} = gA\sin\theta - gA\cos\theta\frac{\partial h}{\partial x} - gAS_f \quad (2)$$

Eq. (1) and (2) are based on mass conservation and momentum conservation principles respectively; Q is the volume flow rate, and A and h are the flow cross sectional area and the free surface level respectively. θ is the angle of inclination of the channel, and g is the acceleration due to gravity. β is the momentum correction coefficient with a value between 1.03 and 1.07. In a non-Newtonian fluid flow, the internal frictional shearing stresses dominate; the frictional slope S_f is then given by [8]:

$$S_f = \frac{\tau_y}{\rho g R_h}\left[1 + \left(\frac{(\epsilon+1)(\epsilon+2)|V|}{(0.74+0.656\epsilon)\left(\frac{\tau_y}{K}\right)^{\epsilon} R_h}\right)^{\frac{1}{\epsilon+0.15}}\right] \quad (3)$$

where $V = Q/A$ is the average flow velocity. $\epsilon = \frac{1}{n}$; ρ, τ_y, K and n are the fluid properties denoting the density, yield shear stress, fluid behaviour index and fluid constituency index respectively. When the wall frictional stresses are significant, the frictional slope is obtained by [8]:

$$S_f = \frac{n_T V}{{R_h}^{2/3}} \quad (4)$$

where n_T is the total roughness coefficient and $R_h = \frac{A}{P_{wet}}$ is the hydraulic radius at each cross section. When the fluid is Newtonian, $n_T = n_M$; n_M is Manning roughness coefficient.

Steady state scheme-ODE form

At steady state, $\frac{\partial A}{\partial t} = 0$, $\frac{\partial Q}{\partial t} = 0$ and then $Q = constant$. Simplifying eq. (2) yields

$$V\beta\frac{dV}{dx} + g\cos\theta\frac{dh}{dx} = g(\sin\theta - S_f) \quad (5)$$

Differentiating the continuity equation $Q = AV$ with respect to x gives

$$V\frac{dA}{dx} + \frac{AdV}{dx} = 0 \quad (6)$$

Assuming a trapezoidal channel with side slope m, $A = (mh + b)h$, and

$$\frac{dA}{dx} = B\frac{dh}{dx} + ch \quad (7)$$

where $c = \frac{db}{dx}$; $B = 2hm + b$ is the top width of the flow, and b is the bottom width at a given section of the flow. Combining eq. (5), (6) and (7) yields:

$$\frac{dh}{dx} = \frac{gAS + \beta chV^2}{gA\cos\theta - \beta BV^2} \quad (8)$$

where $S = \sin\theta - S_f$. The denominator of eq. (8) determines the condition and behaviour of the flow. The critical flow occurs when:

$$gA\cos\theta - \beta BV^2 = 0 \tag{9}$$

The depth of the flow which satisfies eq. (9) is the critical depth. The open channel flow is generally characterized by the Froude number which is expressed as the ratio of flow velocity to the gravity wave celerity, i.e. $Fr = \frac{V}{\sqrt{\left(\frac{gA}{B}\right)}}$ [3]. When $Fr < 1$, the flow is subcritical and when $Fr > 1$, the flow is supercritical. The flow condition is near critical when $Fr \approx 1$. This suggests that eq. (8) can be used to simulate both subcritical and supercritical flow conditions, and also the transition between the two extremes.

Unsteady state scheme

In this paper, we base the numerical scheme for the unsteady state equations (1) and (2) on the finite volume method with staggered grids. With the staggered grid arrangement, the varying slope of the liquid surface is captured [9]. Figure 1 shows the grid arrangement. The node of control volume for momentum conservation is indicated by the line **P** where the velocity is stored. The boundaries of the velocity control volume indicated by the lines **w** and **e** correspond to the nodes of the control volumes for mass conservation, where the depths of the liquid surface are stored. The grid is uniform with spatial spacing, Δx.

Scheme for volume conservation

Spatial integration of eq. (1) over the mass conservation control volume gives

$$\frac{dA_i}{dt} = -\frac{Q_{i+1/2} - Q_{i-1/2}}{\Delta x} \tag{10}$$

To ensure there is no negative depth in the flow, the depths at the boundaries are obtained according to the first order upwind rule [7, 10]:

$$h_{i+1/2} = \begin{cases} h_i, ; & Q_{i+1/2} \geq 0 \\ h_{i+1}; & Q_{i+1/2} < 0 \end{cases} \tag{11}$$

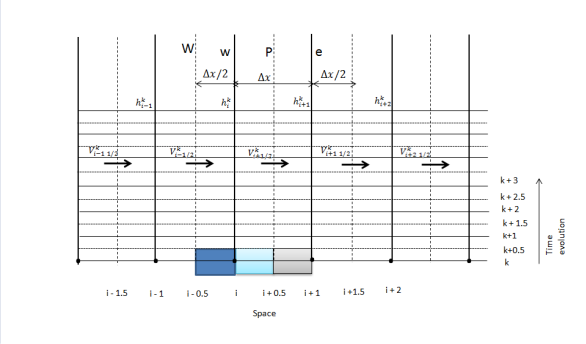

Figure 1: Staggered grid arrangement for V and h control volumes.

Scheme for momentum conservation

Here, the spatial integration of the free surface depth gradient is approximated by the central differencing method, and the flux term is approximated by first order upwind [9]. Over the velocity control volume, the integration of eq. (2) gives

$$\frac{dQ_{i+1/2}}{dt} = -\beta\frac{(QV)_{i+1} - (QV)_i}{\Delta x} - g\bar{A}_{i+1/2}\cos\theta\frac{h_{i+1} - h_i}{\Delta x} + g\bar{A}_{i+1/2}S_{i+1/2} \tag{12}$$

The boundary discharge, Q_i of each cell can be computed as the average value of the neighboring nodes values. The areas at the nodes $\bar{A}_{i+1/2}$ are computed with the average depth measured at the boundaries of the cell [7]:

$$Q_i = \frac{Q_{i+1/2} + Q_{i-1/2}}{2} \tag{13}$$

$$\bar{A}_{i+1/2} = f\left(\frac{h_{i+1} + h_i}{2}\right) \tag{14}$$

The value of flux, $(QV)_i$ can be estimated by the following upwind conditions:

$$(QV)_i = \frac{Q_{i+1/2}+Q_{i-1/2}}{2}\begin{cases} V_{i-1/2}; & \frac{Q_{i+1/2}+Q_{i-1/2}}{2} \geq 0 \\ V_{i+1/2}; & \frac{Q_{i+1/2}+Q_{i-1/2}}{2} < 0 \end{cases} \quad (15)$$

The stability of the scheme described by eq. (10) through eq. (15) depends on the ODE solver for its implementation. The accuracy is only of first order since the scheme is based on first order upwind conditions.

Steady state scheme-discretized form

Considering a positive flow in a trapezoidal channel, from eq. (12) the steady state solution is derived.

$$-\beta\frac{(QV)_{i+1}-(QV)_i}{\Delta x} - g\bar{A}_{i+1/2}\cos\theta\frac{h_{i+1}-h_i}{\Delta x} + g\bar{A}_{i+1/2}S_{i+1/2} = 0$$

$$h_{i+1} = h_i + \frac{1}{\cos\theta}\left(\frac{\beta Q^2}{g(\bar{A}_{i+1/2}*\bar{A}_{i-1/2})} - \frac{\beta Q^2}{g\bar{A}_{i+1/2}{}^2} + \Delta x S_{i+1/2}\right) \quad (16)$$

where

$$\bar{A}_{i+1/2} = \frac{1}{4}(h_{i+1}+h_i)^2 cot\alpha + \frac{1}{2}(h_{i+1}+h_i)b$$

$$\bar{A}_{i-1/2} = \frac{1}{4}(h_{i-1}+h_i)^2 cot\alpha + \frac{1}{2}(h_{i-1}+h_i)b \quad (17)$$

for $i = 1,2,3,\dots,N+1$

Boundary and initial conditions

In the numerical scheme governed by eq. (10), (12) and (16), we consider only subcritical flow conditions. With the use of staggered grids, physical boundaries coincide with scalar control volume (mass conservation) boundaries, and then additional nodes surrounding the domain boundaries are required to store the scalar boundary values [9]. As shown in figure 2, the inlet flow rate Q_{in} is stored at the domain boundary located at $i = 1/2$, and the inlet depth h_{in} is stored at $i = 0$. The outlet values, Q_{out} and h_{out}, are also located accordingly as given in the figure.

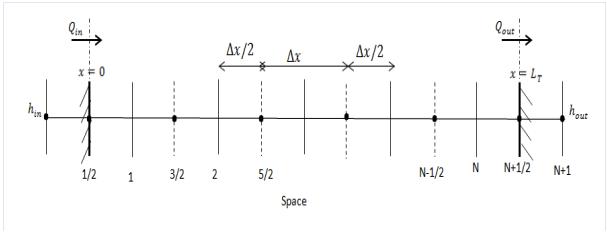

Figure 2: Position of h and Q cells at the domain boundaries.

The values of h at the physical boundaries are obtained by the upwind method, that is $h_{1/2} = h_{in}$ $h_{N+1/2} = h_{out}$. With $Fr < 1$, both boundaries must be specified (Q_{in} and Q_{out} or h_{in} and h_{out}). The numerical solution is based on the so-called backwater curve, implying that the scheme is solved backwards along the domain as indicated in figure 3.

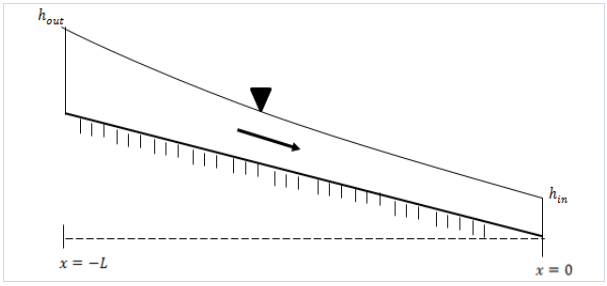

Figure 3: Boundary conditions for computing subcritical flow.

The initial conditions are the values of h and Q at time zero over the entire domain, $i = 1,2,3,\dots,N$. Initial values are often used to initialize the iterations for a system with fully defined boundary conditions, and it depends on specific flows. A steady state solution, h^0 and Q^0, can be assumed as the initial values.

VERIFYING THE NUMERICAL SCHEME

The results obtained from the numerical scheme developed here are in good agreement with the results documented in the literature [6]. Water flow with a steady state flow rate, $Q = 4\,m^3/s$ through a trapezoidal channel: bottom width, $b = 3.5\,m$, side slope $m = 1.5$, length, $L = 1000\,m$, bottom slope, $\theta = 0.05730\,deg$ and Manning's roughness coefficient, $n_M = 0.015$, was simulated for three different levels at the downstream boundary (initial conditions): $h_0 = 1.0,\ 0.664\ and\ 0.4$ m. Figure 4(b) shows the result obtained for the described channel using the steady state eq. (16). Comparing with figure 4(a), it shows that the numerical scheme presented here yields results which are in good agreement with those accepted in literature. Both results are typical of flow profiles for subcritical flow conditions in a uniform channel. It can be seen in the figures that the flow approaches the normal depth $h_n = 0.664$m provided that the flow depth at the inlet is greater than or equal to the critical depth, $h_c = 0.4$m.

FLOW PROFILE IN A RECTANGULAR VENTURI CHANNEL

The Venturi flume simulated here is taken from [11]. The flume geometry is given in figure 5. The data used are the experimental data contained in [12] for studying behaviour of non-Newtonian fluids in open channel flow using a straight rectangular channel of width 300mm. The extracted data are those of kaolin- and bentonite-based fluids with properties and channel bottom slopes shown in table 1. Each pair of the experimental data (Q and h) are only used to establish the initial conditions for simulating the steady state model described by eq. (6), (7) and (8). Figure 6 shows the flow profile for fluids III and IV shown in table 1. The scheme was simulated in MATLAB using ode23. The upper plots in figure 6 give the variation of the level, and the lower plots are the profile of the Froude number associated with the flow along the channel. Figure 6(a) shows that hydraulic jump occurs at the contraction, transiting the flow from supercritical to subcritical conditions. It can also be seen in figure 6(a) that the flow passes through a critical depth in the throat. Figure 6(b) shows that fluid IV with high flow rate accelerates steadily in the channel, and as it can also be seen the channel contraction is not large enough to

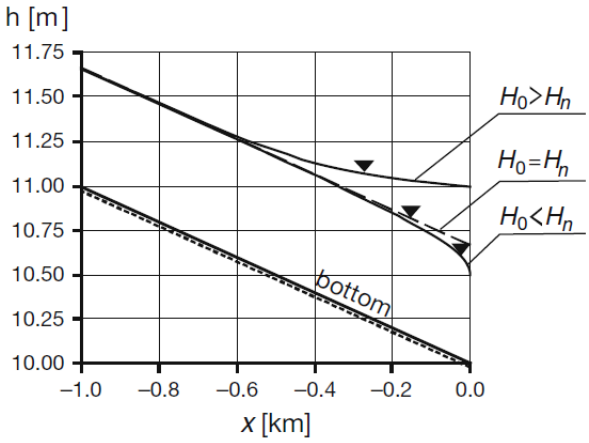

(a)

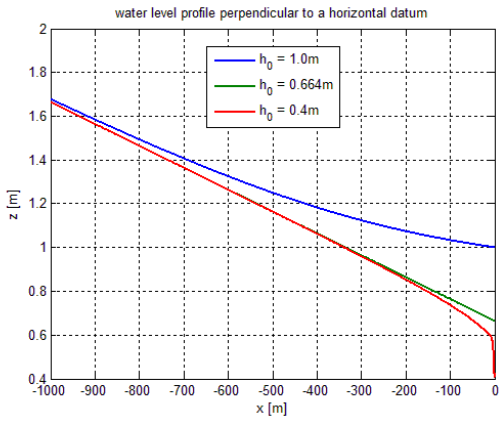

(b)

Figure 4: Steady gradually varied flow level profile in a uniform trapezoidal channel; (a) Result presented in [6]. (b) Result obtained with eq. (16).

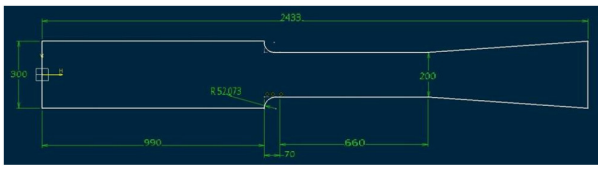

Figure 5: Flume dimension [11].

Properties	Fluids			
	Bentonite -based	Kaolin-based		
	I	II	III	IV
ρ (kg/m^3)	1025	1118.5	1087.1	1098.5
τ_y (Pa)	5.410	10.551	4.985	6.84
K (Pa.s^n)	0.004	0.834	0.03	0.148
n	1.000	0.387	0.717	0.517
channel slope (degree)	2	4	2	3

Table 1: Properties of non-Newtonian fluids for flow simulation [12].

cause a hydraulic jump in the flow. Figure 7 shows the flow profiles of fluids III and IV in the channel when the throat width is reduced to $b = 0.085m$. The result in figure 7(b) shows that increasing the contraction of the channel, the high viscous fluid can transit from supercritical to subcritical flow conditions as expected within the channel. Figure 7(a) shows also that as the contraction is increased the height of the hydraulic jump at the channel contraction increases and the position of the critical depth at the throat is extended.

FLOW RATE MODEL

As can be seen in figure 7, when a sufficient contraction is introduced in a channel, a supercritical flow transits to subcritical flow condition over a relatively large area of the throat. If the flow passes through a critical depth within the throat, a unique relationship between the steady state flow rate and the level measured at a point where the flow is subcritical is established. As given in [5], the flow rate can then be estimated using the same model applicable to subcritical flume.

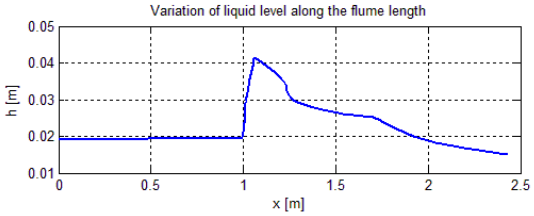

(a) Fluid III: $Q = 3.644l/s$.

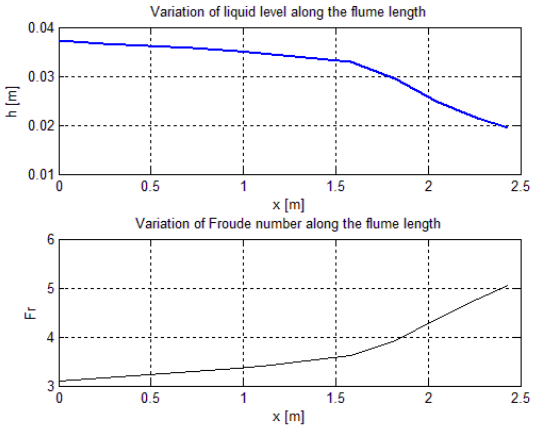

(b) Fluid IV: $Q = 20.821l/s$.

Figure 6: Steady gradually varied flow profiles with a supercritical upstream flow in a rectangular flume: $b = 0.2m$.

For a rectangular flume, the model is described as follow:

$$Q = \left(\frac{2}{3}\right)^{1.5} C_d \, C_v \sqrt{\frac{g}{\alpha}} \, b h_m^{1.5} \qquad (18)$$

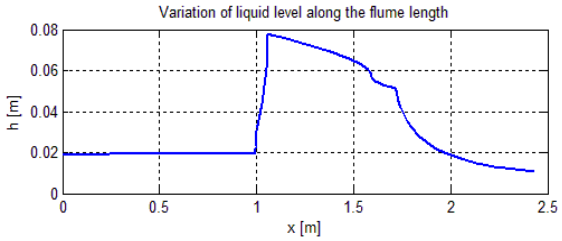

(a) Fluid III: $Q = 3.644l/s$.

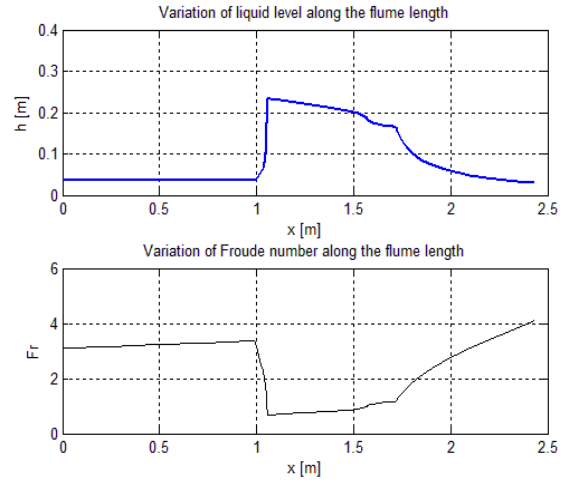

(b) Fluid IV: $Q = 20.821l/s$.

Figure 7: Steady gradually varied flow profiles with a supercritical upstream flow in a rectangular flume: $b = 0.085m$.

where C_d is the coefficient of discharge accounting for losses, and C_v is the coefficient correcting the replacement of the specific energy at the measuring point with the measured depth, h_m. b is the width of the throat, and α is the average kinetic energy correction factor. C_d and C_v are given by:

$$C_d = (1 - 0.006L/b)(1 - 0.003L/h_m)^{3/2} \quad (19)$$

$$C_v = \left(1 + \frac{\alpha}{2gh_m^3}\left(\frac{Q}{b}\right)^2\right)^{1.5} \quad (20)$$

where L is the length of the throat. Since the width of the throat is uniform and the flow within the throat before critical depth is subcritical, the level can be measured in the throat.

RESULTS AND DISUSSION

The model described by eq. (18) was used to estimate the steady state flow rate, and the response of the system to any slight deviation from a steady state was studied using the unsteady state numerical scheme given by eq. (10) and (12).

Estimation of flow rate

Figure 8 shows the simulated flow rate compared with the real flow rate at different measured levels in each of the fluid conditions I and II given in table 1. The values of level used were simulated from the steady state scheme, eq. (8) at the position 1/4th of the throat length from the throat entrance. It can be seen that the simulated flow rates in both fluids show very good agreement with the real flow rate. The results were obtained with some calibration of the model using α as the only tuning parameter. The value shown against each plot of figure 8 shows that α depends on the fluid and on the channel contraction. α also corrects the simulated flow rate for deviations due to inaccurate estimation of the discharge coefficient.

Dynamic behaviour

Since the expected flow condition within the throat of the testing channel is subcritical, the algorithm for unsteady state solution presented here can be performed between the entrance of the throat and the downstream where the flow is critical. The flow rate at the inlet and the

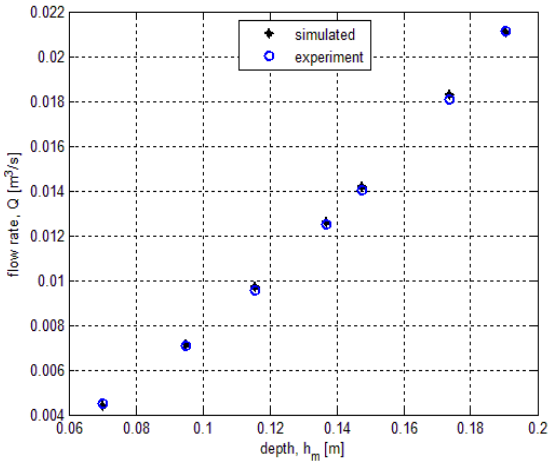

(a) Fluid I: $b = 0.11m$; $\alpha = 1.03$.

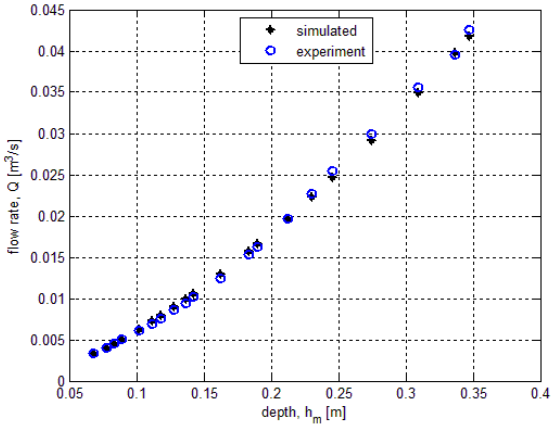

(b) Fluid II: $b = 0.087m$; $\alpha = 0.98$.

Figure 8: Comparing the simulated flow rate with the real flow rate in a Venturi channel.

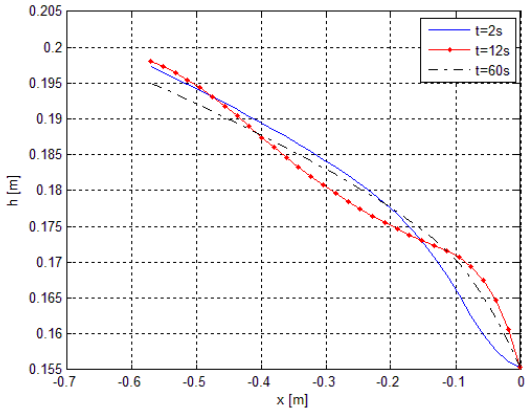

(a) Fluid I: Flow profiles at different time.

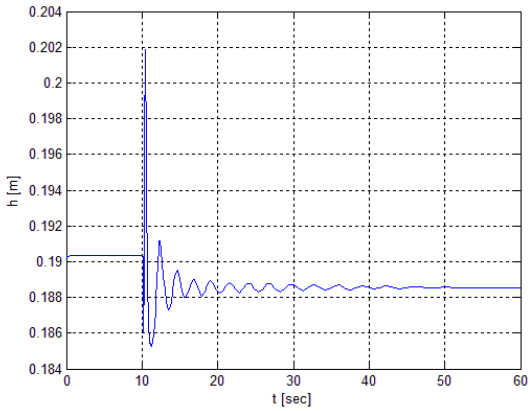

(b) Fluid I: Time evolution of measured depth, 22nd cell.

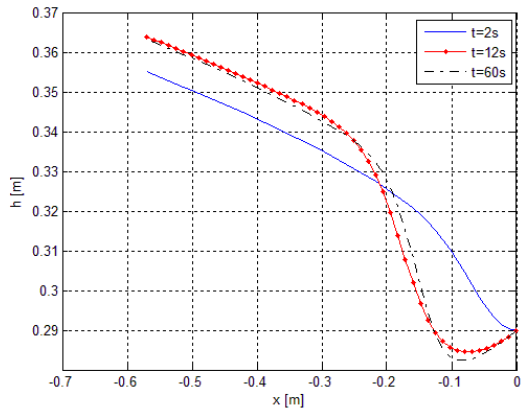

(c) Fluid II: Flow profiles at different time.

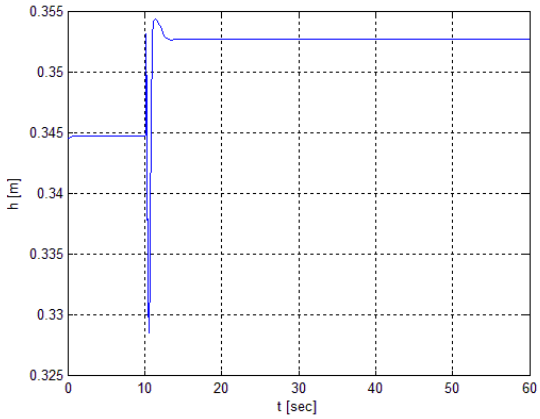

(d) Fluid II: Time evolution of measured depth, 37th cell.

Figure 9: Unsteady state solution for a step change in the flow rate.

corresponding critical depth were the two boundary conditions. The steady state solution based on the boundary flow rate was used as the initial condition. The results shown in figure 9 gives the dynamic response of the flows for fluids I and II with steady state flow rates $Q = 21.137\, l/s$ and $Q = 42.539\, l/s$, and a step change in the flow rate -1.0 and 2.0 l/s respectively. The step change was applied after 10 seconds in each case. The left side plots of figure 9 show the free surface level profile at three time instances, and the right plots show the corresponding time evolution of the level at the measured position for the two cases. As can be seen in figure 9(a and c), the solution of the unsteady state lies within the point of level measurement. The levels before 10 seconds correspond to the steady state values as can be seen by comparing figures 8(a) with 9(b), and 8(b) with 9(d). The values shown in figure 9(d) is slightly lower, and this is due to the size of the grid used. Using the levels in each flow at the end of the simulation run time where the flow is steady, the corresponding simulated flow rates are $20.08\, l/s$ and $42.80\, l/s$ representing accuracy of 0.28% and 3.9% respectively in using the unsteady state scheme for flow rate estimation in a dynamic system. As can be seen in figure 9(d), the system reaches a new steady state corresponding to the new flow rate in less than 5 seconds after the step change is applied with few oscillations. However, with a sudden decrease in the flow rate (fluid I), the system oscillates quite long before reaching a steady state. The systems were simulated in MATLAB using ode15s with spatial grid sizes 30 and 50 respectively. The major challenge in achieving the results was locating the critical depth in the throat.

CONCLUSION

In this paper we investigated the possibility of using a Venturi channel to estimate the flow rate of a non-Newtonian fluid in an open channel. Non-Newtonian fluid flow behavior was studied using the one-dimensional Saint Venant equation. The analysis was based on the supercritical upstream flow condition in the channel. We found that both channel contraction and the fluid apparent viscosity are critical parameters that determine the fluid flow behavior in the channel, and when there is a sufficient contraction to cause flow jump to subcritical levels within the throat, the standard specific energy model can be used to simulate a steady state flow rate. The results showed that the simulated flow rate is in a good agreement with the real flow rate when the model is properly tuned. Also, the dynamic response of the system for a slight deviation of steady state values was studied, and the results showed that the scheme we presented here is stable within some degree of accuracy, and capable of predicting the system response, reaching the steady state solution within the simulation run time. We will investigate the optimum channel contraction and throat length for a supercritical Venturi flume in our future work.

ACKNOWLEDGEMENT

The support from Statoil ASA, the Intelligent Drilling group by Bjørn Rudshaug, is gratefully acknowledged.

REFERENCES

[1] Balmforth NJ, Craster RV. *Geophysical aspects of non-Newtonian fluid mechanics*. Geomorphological Fluid Mechanics 2001; LNP 582: 34 - 51.

[2] Ministere du Developpment durable, de L'environment et Desparcs du Que'bec (2007). *Sampling guide for environmental anlysis: booklet 7 - flow measurement methods in open channels*. May 2007, Centre d'expertiseen analyse environmentale du Que'bec, 223p.

[3] Wilson KC. *Flume design for homogeneous slurry flow*. Particulate Science and Technology 1991; 9: 149-159.

[4] Smith RE, Chery DL, Renard Jr KG, Gwinn WR. *Supercritical flow flumes for measuring sediment-laden flow,* Bulletin No. 1655, 72 p. Illus: U.S. Department of Agriculture Technical, 1981.

[5] ISO 4359: 2013(E). *Flow measurement structures-rectangular, trapezoidal and U-shaped flumes*. Switzerland: International Standard, 2013.

[6] Szymkiewicz R. *Numerical modeling in open channel hydraulics (Vol.83),* Springer, ISBN 978-90-481-3673-5, 2010.

[7] Aldrighetti E. *Computational hydraulic techniques for the Saint Venant equations in arbitrarily shaped geometry*, PhD thesis. Trento, Italy: Universit`a degli Studi di Trento, 2007.

[8] Jin M, Fread DL. *One-dimensional routing of mud/debris flows using NWS FLDWAV model, in Debris-Flow Hazards Mitigation: Mechanics, Prediction, and Assessment*, Edited by Chen-lung Chen, ASCE, New York, 1997: 687–696.

[9] Versteeg HK, Malalasekera W. *An introduction to computational fluid dynamics: finite volume method*, 2nd ed. England: Pearson Education Limited, Edinburgh Gate Harlow Essex CM20 2JE, 2007.

[10] Stelling GS, Duinmeijer SPA. *A staggered conservative scheme for every Froude number in rapidly varied shallow water flows*. International Journal for Numerical Methods in Fluids 2003; 43: 1329 - 1354.

[11] BAMO Measure. *Flow rate measurement in open channel: DF 2500 Instructions manual*. Argenteuil: BAMO Control Ltd., 2009.

[12] Haldenwang R. *Flow of Non-Newtonian Fluids in Open Channels*, PhD thesis. Cape Town, South Africa: Cape Technikon, 2003.